ACS APPLIED ENERGY MATERIALS

Article

www.acsaem.org

Microwave Processed, Onionlike Carbon and Fluoropolymer Passivated Lithium Metal Electrode for Enhanced Li Stripping/Plating Performance

Kewei Liu,[†,§] Yanfeng Xia,[‡,§] Chung-Fu Cheng,[†] Xuhui Xia,[‡] Feng Zou,[†] Bryan D. Vogt,[*,‡,∥] and Yu Zhu[*,†]

[†]Department of Polymer Science, University of Akron, Akron, Ohio 44325, United States

[‡]Department of Polymer Engineering, University of Akron, Akron, Ohio 44325, United States

Supporting Information

ABSTRACT: One key limitation of lithium metal electrodes is their propensity for dendrite formation that limits their use in commercial batteries. Here, a simple surface modification method was demonstrated to improve the electrochemical stability of the lithium metal electrode through direct coating of onionlike carbon (OC) and fluoropolymer onto the lithium metal electrode. Selective and rapid microwave heating of the OC resulted in the *in situ* formation of a LiF-rich composite with the simultaneous infiltration of lithium into the OC. The electrochemical stability of the modified electrode was compared with a neat lithium metal electrode with symmetric stripping/plating cells. The microwave processed surface coating acted as a robust and stable passivation layer to prevent electrolyte decomposition, while also suppressing fast dendrite growth. The potential stability during the stripping and plating was enhanced at all rates examined (0.5−2 mA/cm^2). With the stripping/plating capacity of 1 mA h/cm^2, the microwave processed lithium metal electrode can be cycled over 1000 h at a current density of 0.5 mA/cm^2. These results demonstrated that microwave treatment is a promising method for selective modification of the lithium metal electrode to improve its performance in energy storage applications.

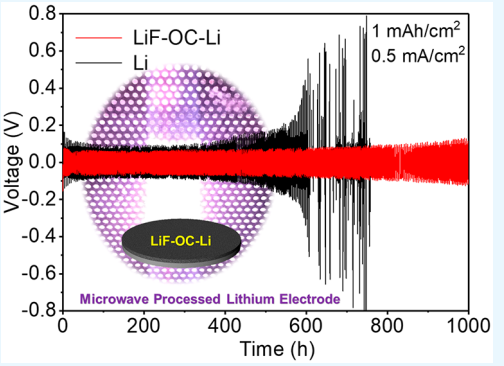

KEYWORDS: *lithium metal anode, onionlike carbon, microwave, lithium metal battery, fluoropolymer*

1. INTRODUCTION

Advances in lithium ion batteries (LIBs) have enabled the expansion in mobile electronics and their performance over the past decades, but the anodes of these LIBs have been based on carbon materials that are rapidly approaching their theoretical capacities[1−5] in commercialized cells. The conventional graphite anode is based on an intercalation mechanism, which limits the Li ion storage capacity and results in a relatively low gravimetric energy density.[6] The ever-growing need for higher energy densities to facilitate high-power-consumption mobile devices and electric vehicles has driven research into exploring chemistries for new electrode materials. For LIBs, Li metal represents the ideal anode material with a capacity of 3860 mA h/g and the lowest negative electrochemical potential possible.[7,8] Although the use of alloying (e.g., Si, Sn, Ge)[9−11] or conversion reactions (e.g., metal oxide, metal sulfide)[12−14] can significantly increase the specific capacity as well, their electrochemical potentials are higher than lithium or graphite, leading to the undesired trade-off between cell voltage and capacity. In addition, beyond-LIB systems (Li-oxygen and Li-sulfur) with potentially even higher energy densities[15−18] rely on Li metal anodes.

However, there are great challenges to make Li metal anodes commercially viable. The repeated removal and redeposition of Li metal lead to continual roughening of the surface. The uneven Li deposition culminates in the formation of dendrites.[19] The growth of dendrites also generates a new exposed Li surface to consume additional electrolyte through the formation of a solid electrolyte interface (SEI) layer on the newly exposed Li.[20−25] Additionally, the early stages of dendrite formation and growth generate porous and rough structures at the Li anode. This morphology increases the ion diffusion path length and effective resistance of the anode, which increases the required overpotential to drive the Li stripping/plating associated with charging/discharging.[26−30]

Significant efforts have been dedicated to developing routes to suppress dendrite growth, including the design of special electrolytes[31,32] and the surface modification of the Li anode.[28,33] The rationale associated with electrolyte modification relies on the formation of a robust and highly ionic conductive SEI layer that can effectively mitigate the

Received: July 21, 2019
Accepted: October 31, 2019
Published: October 31, 2019

DOI: 10.1021/acsaem.9b01416
ACS Appl. Energy Mater. XXXX, XXX, XXX−XXX

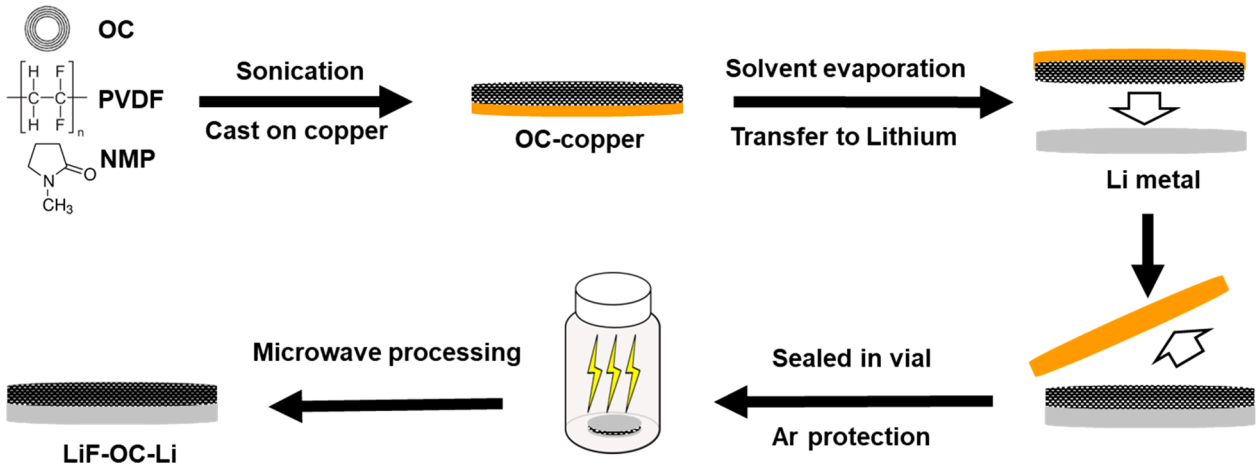

Figure 1. Schematic illustrating the preparation process of the LiF-OC-Li electrode. OC/PVDF/NMP slurry was cast on copper foil and dried. The OC-PVDF film was compressed on Li to achieve a free-standing OC-PVDF-Li electrode. Microwaves transform the OC-PVDF-Li electrode to the LiF-OC-Li electrode.

nucleation and growth of dendrites. A variety of additives, such as KNO_3,[34] LiODFB,[35] LiBOB,[36] $AlCl_3$,[37] and Li polysulfides,[38−40] have been shown to improve the ionic conductivity of the SEI,[41,42] while selection of nontraditional electrolytes, such as ceramic ion conductors,[43,44] polymer electrolytes,[45−47] and superconcentrated electrolytes,[48−51] can improve the mechanical strength and electrochemical stability of the electrolyte layer to mitigate dendrite growth and various side reactions. Alternatively, methods to confine Li within conductive 3D matrixes on the anode were reported to suppress dendrite growth. Such matrix materials include graphene derived matrix,[52−54] graphene−CNT hybrid material,[55] porous carbon films,[56,57] Cu/Ni foam,[58,59] and Li_7B_6 frameworks.[60,61] In the examination of cases where a stabilized lithium anode was demonstrated, LiF was often reported as an active ion-conducting material in the robust artificial SEI, due to its excellent chemical stability and low solubility in carbonate-based electrolytes.[33,62] However, the direct deposition of the LiF on the Li anode is a tedious process and requires special capabilities.[63,64] Here, a simple and efficient method was developed to fabricate a LiF decorated Li metal electrode through localized microwave heating of onionlike carbon (OC) and PVDF decorated Li foil. Microwaves were efficiently absorbed by the OC to lead to lithium infiltration into the OC and thermal decomposition of PVDF. The degradation of the PVDF leads to *in situ* formation of a LiF-rich composite at the surface of the Li electrode (LiF-OC-Li). The LiF-OC-Li electrode exhibited improved stability in stripping plating tests as compared to neat Li electrodes. This microwave processed artificial passivation layer is a promising methodology to facilitate safe lithium metal electrode implementation in rechargeable batteries.

2. EXPERIMENTAL SECTION

Materials. Lithium hexafluorophosphate ($LiPF_6$, battery grade, Oakwood), lithium foil (15.6 mm in diameter and 0.25 mm in thickness, MTI Corporation), ethylene carbonate (EC, 99.9% Sigma-Aldrich), diethyl carbonate (DEC, 99% Sigma-Aldrich), and *N*-methyl-2-pyrrolidone (NMP, 99.5% EMD) were utilized as received. Other materials were purchased from VWR and used as received.

Preparation of the OC. The OC was synthesized by hydrothermal processing of phenolic resin (resol), tetraethyl orthosilicate (TEOS), Pluronic F127, and trimethylbenzene (TMB), following a prior published report.[65] Briefly, 1.0 g of Pluronic F127 was dissolved with 6.25 g of resol in 20 wt % ethanol solution[66] and 1.0 g of TMB under magnetic stirring at 25 °C for 1 h to obtain a clear solution. Simultaneously, 2.34 g of TEOS was hydrolyzed using 150 mL of 1.0 M HCl at 40 °C for 30 min. The dissolved F127/resol solution was then added dropwise to the TEOS solution under continuous stirring for 12 h at 400 rpm at 40 °C. Subsequently, the solution was transferred to the Teflon chamber of a hydrothermal autoclave reactor (50 mL). The sealed autoclave was heated at 90 °C for another 24 h. The solid raw products from the autoclave were filtered and washed repeatedly using deionized (DI) water until the pH of 7 is reached. The sample was then left to dry in air until no obvious water was visible. The dried materials were carbonization at 800 °C for 1 h under N_2 protection in a ceramic tube furnace. The silica in the carbonized powder was subsequently etched with 6 M KOH solution (ethanol:H_2O = 50:50 v/v) for 24 h at 90 °C. The resultant mesoporous carbon was washed by deionized water over 20 times using Soxhlet extraction to completely remove the residual KOH and was dried in an oven at 80 °C.

Preparation of the LiF-OC-Li Electrode. A 22 mg portion of OC was dispersed in 1.5 mL of PVDF solution (1.6 mg/mL in 1.5 mL NMP) in an Ar-filled glovebox. After 20 min of sonication, a 55 μL OC suspension was drop-cast onto the smooth side of a Cu chip (diameter 1/2 in.) that was then dried at 80 °C overnight in an Ar glovebox. (The smooth side of the Cu chip was employed for the OC film coating to allow for the Cu to be removed in the next step.) The OC-PVDF coated side of the Cu chip was placed onto a Li foil chip (1/2 in. diameter) and compressed at 250 psi with OC-PVDF embedding in the Li under this pressure. The Cu foil was then simply peeled off (like removing a sticker from its backing) to obtain the freestanding OC-PVDF film embedded Li foil chip. Due to the stronger adhesion between the lithium metal and OC-PVDF composite, almost all of the OC-PVDF was transferred to the surface of the lithium foil. The OC-PVDF-Li electrode was punched in a 7/16 in. diameter disk and transferred into a 20 mL vial. An additional Li chip was placed on top of the OC-PVDF-Li electrode without any pressure applied. The vial was sealed and moved into the microwave chamber (BP-210 microwave, Microwave Research and Applications Inc., 2.45 GHz). The composite stack was exposed to 1000 W microwaves for 10 s to transform the OC-PVDF to LiF-OC. After the microwave reaction, the sealed vial was returned to the Ar glovebox. The top Li chip was removed, and the LiF-OC-Li electrode was collected.

Characterization. SEM and TEM images were collected using JEOL JSM-7401F and JEOL 1203 microscopes, respectively. High-resolution TEM (HRTEM) images were obtained using an FEI Tecnai G2 instrument. Nitrogen adsorption/desorption isotherms

DOI: 10.1021/acsaem.9b01416
ACS Appl. Energy Mater. XXXX, XXX, XXX−XXX

were obtained at 77 K using a TriStar II (Micromeritics) instrument. The Brunauer–Emmett–Teller (BET) method was applied to determine the specific surface area in the relative vapor pressure range 0.04–0.27. The adsorption isotherm was utilized to determine the pore size distribution by applying the Barrett–Joyner–Halenda (BJH) model. SAXS measurements using 13.5 keV X-rays were performed on the 11-BM CMS beamline at the National Synchrotron Light Source II (NSLS-II) at Brookhaven National Laboratory in Upton, NY. The sample-to-detector distance was 1.98 m with a Dectris Pilatus 2 M detector (pixel size = 172 μm × 172 μm).

Cell Fabrication and Electrochemical Test. Symmetric stripping plating cells and asymmetric cells for Coulombic efficiency measurements were assembled in an Ar-filled glovebox using 2032 coin cells cases. The oxygen and water contents were controlled below 0.5 ppm. Celgard membrane (MTI) was used as the separator. The electrolyte was 1 M lithium hexafluorophosphate solution in EC and DEC (1:1 v/v). Symmetric cells were assembled by using the LiF-OC-Li (lithium foil thickness: 0.25 mm) or neat Li (lithium foil thickness: 0.25 mm) electrode as both working and counter/reference electrodes. A 25 μL portion of electrolyte was added to the cells via an Eppendorf pipet inside the glovebox. For the Coulombic efficiency test, a thin Li metal chip with a thickness of 50 μm was utilized as the working electrode with a LiF-OC-Li or neat Li electrodes as a counter/reference electrode. Electrochemical impedance spectroscopy (EIS) was collected by using an electrochemical workstation (CHI608E) over a frequency range from 100 kHz to 0.1 Hz, with the open circuit voltage as the perturbation voltage. Galvanostatic charge and discharge tests were carried out using a battery analyzer BST-8A (MTI).

3. RESULTS AND DISCUSSION

The procedure associated with the preparation of the LiF-OC-Li electrode is illustrated schematically in Figure 1. The procedure was described in detail in the Experimental Section. Briefly, PVDF was dissolved in NMP, and the OC was dispersed in this solution, which was drop-cast on polished copper foil. After drying, the OC-PVDF coated copper foil was mechanically compressed on a Li metal electrode. The copper foil was then peeled to produce a freestanding OC-PVDF-Li metal electrode, which was microwave processed under Ar to produce the LiF-OC-Li electrode.

The OC was synthesized following a previously reported hydrothermal method.[59] A synthetic scheme (Figure 2a) illustrates the process as described in the Experimental Section. The aggregated OC particles were observed by using high-resolution TEM (HRTEM) (Figure 2b). These OCs exhibit a hierarchical structure with ca. 200 nm spherical particles consisting of nanostructured carbon walls separated approximately 15 nm (inset in Figure 2b), which is consistent with expectations for the onionlike multilayered vesicle structure.[59] The spherical particles were derived from the vesicular structure formed by the self-assembly of the Pluronic surfactant around the trimethylbenzene (TMB) during hydrothermal reaction. This self-assembled structure was confirmed by small-angle X-ray scattering (SAXS) (Figure 2c). The scattering pattern exhibits a strong maximum at $q^* = 0.0378$ Å^{-1} and a weak shoulder at $q \triangleq 0.0756$ Å^{-1} ($\triangleq 2q^*$ as expected for a lamellar structure). The spacing associated with the primary peak (16.6 nm) is consistent with the d-spacing determined from HRTEM. Additional information about the pore structure was elucidated from the nitrogen adsorption/desorption isotherms (Supporting Information, SI, Figure S1a). The adsorption isotherm exhibits rapid adsorption at low P/P_0 (<0.10) associated with micropores templated by the etched silica, increased adsorption around $P/P_0 = 0.6$ associated with the mesopores, and further increased

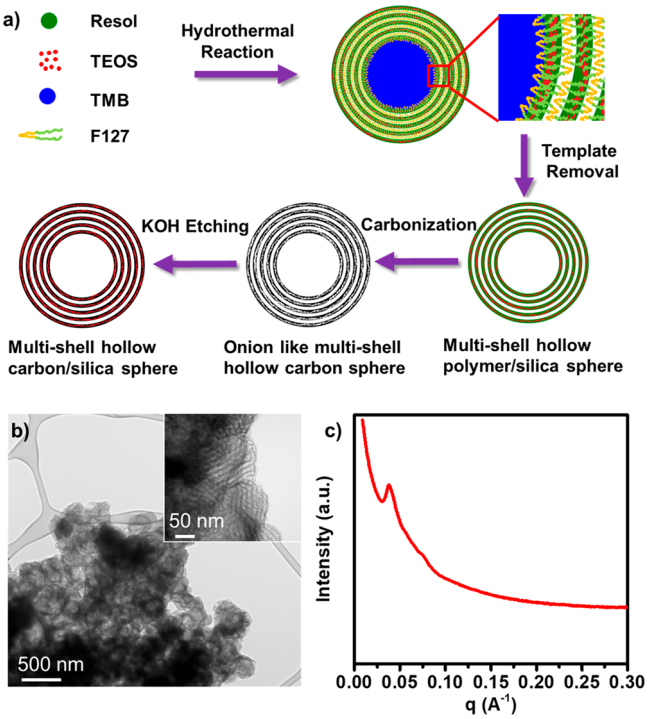

Figure 2. (a) Schematic illustrating the steps involved in the preparation of the OC. Resol, phenolic resin; TEOS, tetraethyl orthosilicate; F127, Pluronic F127; TMB, trimethylbenzene. Structural characterization of the OC material by (b) TEM and (c) SAXS. The inset in part b is HRTEM that illustrates the nanostructure with a common spacing of around 15 nm. This size is consistent with the d-spacing obtained from the primary peak in the SAXS of the OC in part c.

adsorption at $P/P_0 > 0.95$ associated with larger pores formed by the TMB.[59] The hysteresis loop between adsorption and desorption isotherms is consistent with the mesoporous structure. From the adsorption isotherm, the pore size distribution (SI, Figure S1b) was obtained that revealed a large number of small (<2 nm) micropores, a relatively narrow mesopore size centered at approximately 10 nm, and the presence of much larger pores. Due to the instrumental sensitivity, the distribution of large pores could not be accurately quantified from N_2 adsorption measurements. The chemical composition of OC was confirmed by XPS where only C and O peaks are observed (SI, Figure S2).

The OC-PVDF film was transferred to the lithium metal film and treated with microwaves as described in the Experimental Section. Figure 3a1,a2 illustrates the difference in the optical appearance of the modified electrode (LiF-OC-Li) and the neat Li electrode, respectively. The optical appearance of OC-PVDF covered lithium metal film did not change appreciably after the microwave treatment. The black color of the LiF-OC-Li therefore was derived from the OC. However, as shown in Figure 3a3, the sample was glowing during the microwave heating. Lithium metal film used in this experiment is a good conductor and does not possess a large surface area; therefore, it is regarded as a bulk metal for the microwave used in the experiments. During the microwave treatment, the bulk metal had a high degree of microwave reflection, accompanied by the induction of surface eddy currents, leading to the arch discharge.[67,68] The bright light emitted from the sealed reactor confirmed such a process. Both PVDF and OC can efficiently

DOI: 10.1021/acsaem.9b01416
ACS Appl. Energy Mater. XXXX, XXX, XXX–XXX

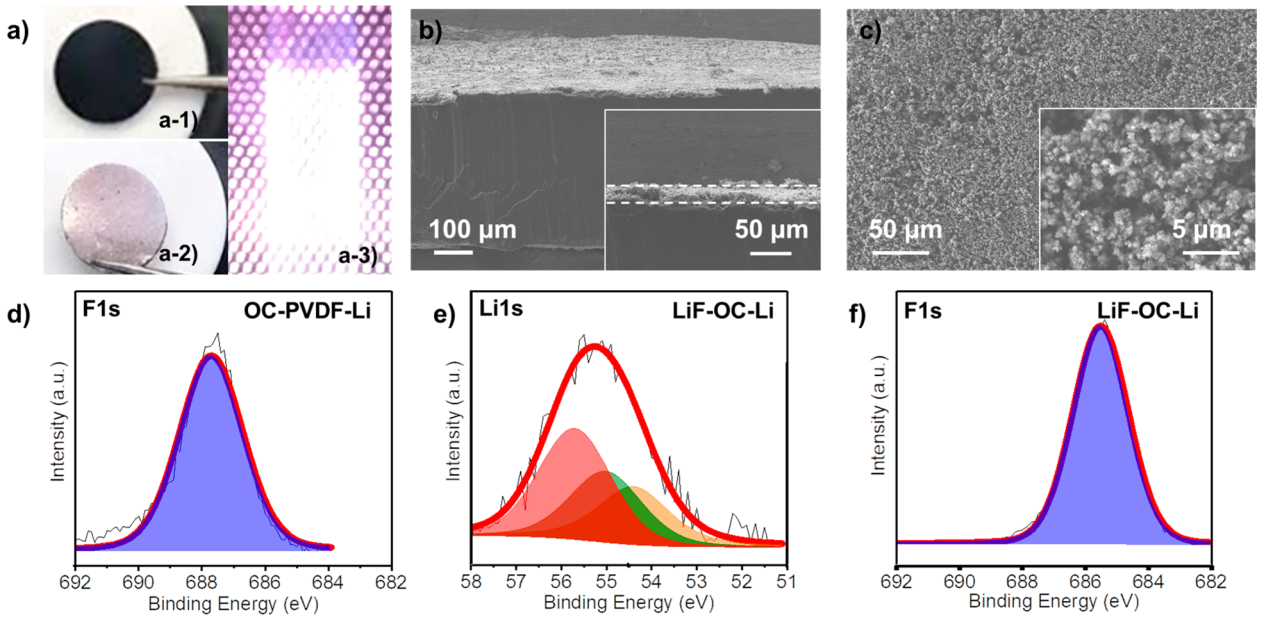

Figure 3. Structural and chemical characterization of the LiF-OC-Li electrode. (a) Optical micrographs of (a1) LiF-OC-Li electrode after microwave treatment, (a2) neat Li chip, and (a3) OC-PVDF film covered Li in the vial during microwave exposure. (b) SEM image of the cross-section of the LiF-OC-Li electrode. The inset shows the thickness of the OC layer (≈30 μm). (c) SEM image of the surface of the LiF-OC-Li electrode with a higher magnification image shown in the inset. High-resolution XPS spectra of (d) the OC-PVDF film covered Li electrode before the microwave process (F 1s spectrum) and the LiF-OC-Li electrode after microwave treatment for (e) Li 1s and (f) F 1s spectra.

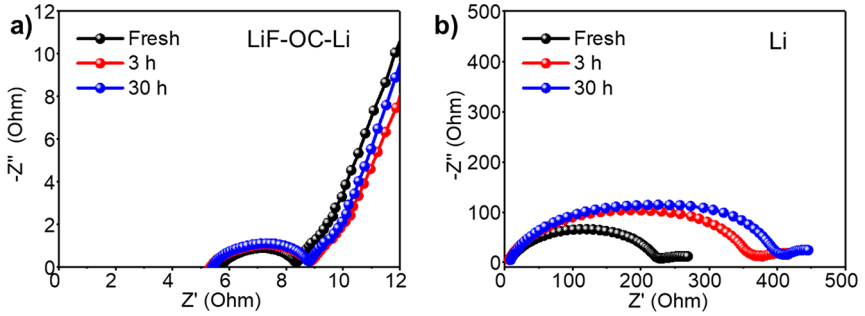

Figure 4. Stability study of the LiF-OC-Li electrode and neat Li metal electrode with impedance spectroscopy. Nyquist plots for (a) LiF-OC-Li and (b) neat Li electrodes at three different resting times demonstrate the influence of the modified layer on the stability of the electrode in 1 M $LiPF_6$ in EC and DEC (1:1 v/v).

absorb microwaves due to the high dielectric loss tangent of carbon material and polar PVDF molecules.[68,69] As OC also possesses a high surface area, which will benefit the absorption of microwave energy, it is believed that OC produced heat to decompose PVDF during the microwave treatment as PVDF alone coating on the Li does not decompose under the same microwave conditions. After the microwave treatment, the cross-section of the LiF-OC-Li electrode was examined. As shown in Figure 3b, this modified layer is approximately 30 μm thick and conformally coated on the surface of lithium metal film. The surface morphology of the LiF-OC-Li electrode was studied by SEM imaging (Figure 3c). The surface particulate morphology is consistent with prior characterization of OC alone,[65] suggesting that the morphology of mesoporous OC remained after the microwave treatment. To understand the chemical changes, X-ray photoelectron spectroscopy (XPS) was utilized to characterize the surface before and after the microwave treatment. Prior to microwave exposure, the surface was predominately covered by carbon with no Li signals (SI, Figure S3a). From the high-resolution scan of F 1s binding energy (Figure 3d), the fluorine can be attributed to the PVDF component with a peak at 687.7 eV.[70] After the microwave reaction, Li can clearly be observed in the survey scan (SI, Figure S3b). The bonding state of the Li was examined in detail using the Li 1s spectrum presented in Figure 3e. Besides the expected Li−O (54.9 eV, green band) and Li−Li (54.3 eV, orange band),[48,71] a clear peak at 55.7 eV (red band) was observed from the deconvoluted spectrum. This peak at 55.7 eV is attributed to Li−F, indicating the formation of LiF during the microwave treatment (Figure 3e).[64] This change of F atom bonding states from PVDF to LiF was also witnessed by the shift of peak position in the F 1s spectra from 687.7 to 685.5 eV (Figure 3f), which has been widely reported as the F−Li bond.[47,64] Based on the characterization results, the suggested mechanism is an extremely fast microwave heating process (10 s) close to the upper layer of the lithium film, where OC materials were quickly heated up and decomposed PVDF. The heat flux also melted the lithium, and capillarity drove the Li into the OC layer, reacting with decomposed PVDF and forming a Li composite with a significant amount of LiF.

DOI: 10.1021/acsaem.9b01416
ACS Appl. Energy Mater. XXXX, XXX, XXX−XXX

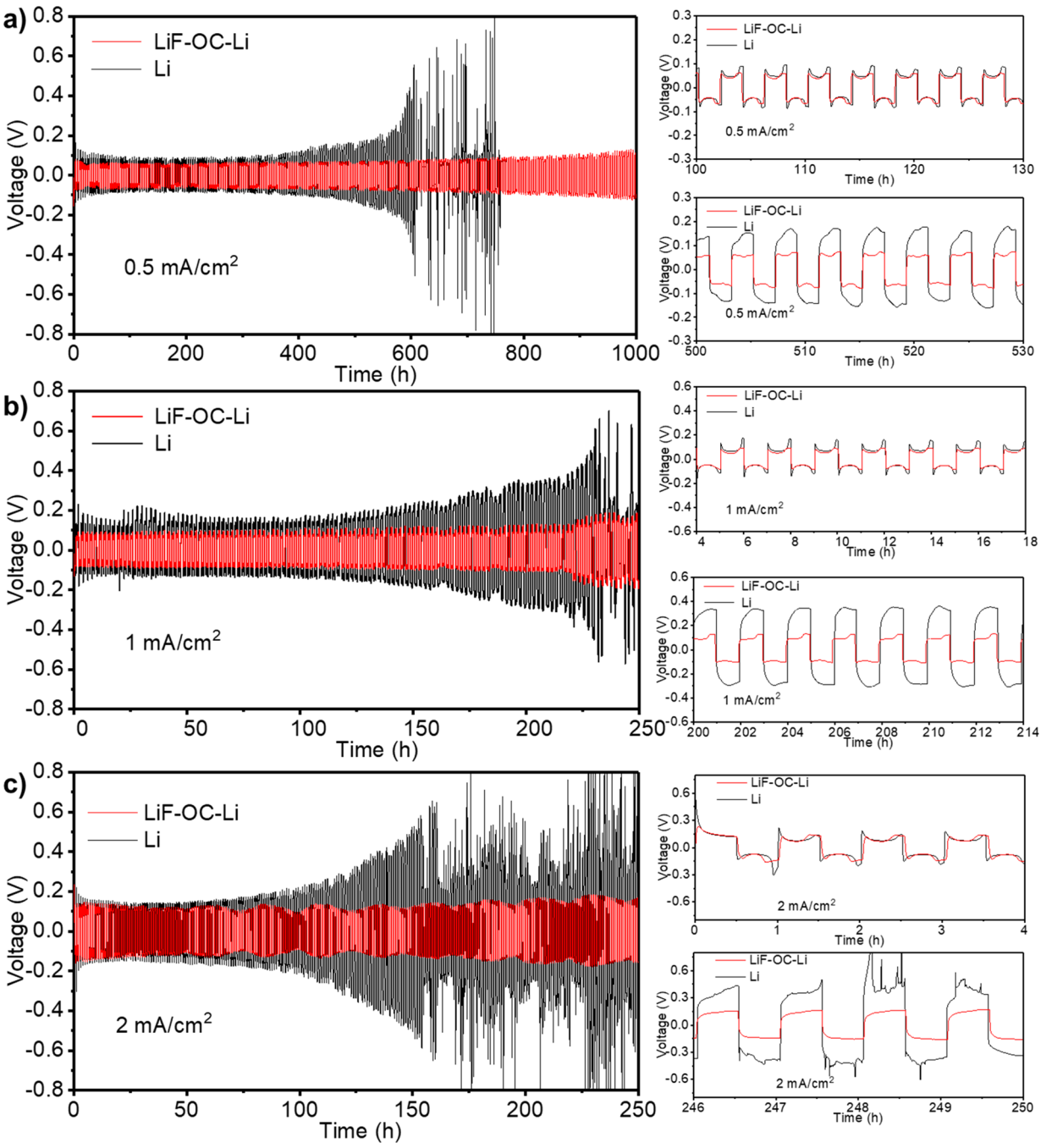

Figure 5. Galvanostatic cycling performance of the LiF-OC-Li and neat Li electrode. Voltage profiles of stripping and plating in a symmetric cell at current densities of (a) 0.5 mA/cm^2, (b) 1 mA/cm^2, and (c) 2 mA/cm^2. The figures on the right show detailed voltage profiles as indicated.

The electrochemical stability tests of the LiF-OC-Li and neat Li metal electrodes were performed using a symmetric coin cell with 1 M lithium hexafluorophosphate ($LiPF_6$) solution in ethylene carbonate (EC) and diethyl carbonate (DEC) (1:1 v/v) as the electrolyte. The evolution in impedance at the open circuit potential over time provides one key measure of stable passivation layer formation on the electrode/electrolyte interfaces. As shown in Figure 4, the initial impedance of the LiF-OC-Li electrode was only 2.8 Ω, which is 2 orders of magnitude smaller than that for the fresh neat Li cell. This result suggested that the LiF-OC surface modification improved charge transfer on the interface between the bulk electrode and bulky electrolyte. More strikingly, the impedance of the LiF-OC-Li only increased slightly as the cell rested. A stable charge transfer resistance (3.3 Ω) was obtained after 1 h of resting without further changes in the following 30 h (Figure 4a). In comparison, the charge transfer resistance of the neat Li electrode increased monotonically (Figure 4b). The LiF-OC acts to protect the Li electrode from side reactions, while a series of side reactions occurred on the neat lithium electrode to form increasing interlayers on the surface of the lithium metal surface.

To confirm the importance of the microwave derived LiF, two control samples were examined. As the OC is highly conductive and porous, this may provide improved electron transport and a tortuous diffusion path that could be beneficial

DOI: 10.1021/acsaem.9b01416
ACS Appl. Energy Mater. XXXX, XXX, XXX−XXX

to the performance. Coating the lithium foil with only OC and treating with the same microwave process as the LiF-OC-Li electrode generates a porous carbon modified surface (OC-Li). Figure S4 illustrates the electrochemical impedance spectra of this electrode for the fresh electrode and after aging in the electrolyte solution for 3 and 30 h. As expected due to the good conductivity of the OC, the initial impedance is smaller for the OC-Li than the neat Li electrode (Figure 4b), but still larger than the LiF-OC-Li (Figure 4a). The lower impedance with the LiF-OC-Li is indicative of the improved charge transport from the LiF between the OC particles on the Li foil. More importantly, the impedance for the OC-Li increases dramatically with the aging in the electrolyte, similar to the neat Li electrode. This suggests that the LiF formed from the microwave-based decomposition of PVDF is critical to the stability of these modified electrodes. To illustrate that the microwave processing was important to achieve the stable electrode, the lithium electrode was coated with OC-PVDF without microwave treatment (OC-PVDF-Li). The OC-PVDF-Li has smaller impedance than the neat Li electrode (Figure 4b), but larger impedance than LiF-OC-Li (Figure 4a) and the OC-Li. The impedance for the OC-PVDF-Li also increases significantly during aging in the electrolyte, similar to the neat Li electrode. These results confirm that the *in situ* formed LiF containing layer acts as a stable SEI layer to protect the Li electrode.[72]

Lithium plating/stripping measurements were carried out to evaluate the performance of the LiF-OC-Li electrode in comparison to the neat Li electrode. Dendrite growth during Li deposition is known to consume the active Li source while also decomposing the electrolyte continuously to form an unstable SEI layer. These effects lead to increased overpotential and battery impedance.[73] Here, examination of the overpotential during plating and stripping of a fixed quantity of Li (1 mA h/cm^2) at constant current density in symmetric cells was used to evaluate the stability of the electrode/electrolyte interfaces. As can be observed in Figure 5, the LiF-OC-Li electrode exhibited a smaller overpotential and less variation in the overpotential during long galvanostatic cycling when compared with the neat lithium electrode. At a current density of 0.5 mA/cm^2, the overpotential of the LiF-OC-Li electrode was initially stable around 60 mV and increased to approximately 95 mV after 1000 h of stripping/plating. In contrast, the neat Li electrode exhibited a larger overpotential initially (160 mV) and increased beyond an acceptable value (550 mV) associated with a cycle life of approximately 600 h (Figure 5a). Similarly at a higher current density of 1 mA/cm^2, larger voltage fluctuations and higher overpotentials were also observed for the neat Li electrode system with respect to the LiF-OC-Li electrode (Figure 5b). Further increasing the current density to 2 mA/cm^2 led to some oscillatory features for the LiF-OC-Li electrode (Figure 5c), but the overpotential after 250 h remained similar to the initial potential. The neat Li electrode, however, lost stability after 100 h of stripping/plating.

The electrochemical impedance spectra of neat Li and LiF-OC-Li were collected after cycles (Figure S5). Those data demonstrate that the impedance for the electrode with the LiF-OC-Li remains small after 20 cycles. There are several mechanisms at play, responsible for the increased stability in the overpotential made evident by the lack of large voltage fluctuations for the LiF-OC-Li electrodes. The conductive, nanostructured OC hosted LiF-rich composites provide a stable interface and fast Li-ion diffusion. Previous work have also reported the increased surface conductivity associated with the LiF containing layers. There could be secondary effects from the increased tortuosity on the surface of the lithium electrode modified by OC particles to promote uniform deposition of Li. The porous carbon structure may help to prevent the formation of a large dendritic crystal, leading to a smoother lithium layer deposition during the cycling tests.[74]

These differences were also manifested in the changes of surface morphology of the electrodes after 250 h of cycling at 1 mA/cm^2 as shown in Figure 6. The morphology of the LiF-OC-Li electrode surface after cycling (Figure 6a) is very similar to the fresh electrode (Figure 6c), whereas the neat Li electrode evolved from a relatively featureless surface morphology (Figure 6b) to "mossy" Li (Figure 6d).[20] The cross-section images of the LiF-OC-Li electrode are shown in the SI. As shown in Figure S6, the thickness of the LiF-OC layer was not significantly changed as compare with its initial state (Figure 3b). However, the cross-section image of the neat lithium electrode showed a rough surface morphology, and the edge of the top surface layer was unclear in the micrograph, indicating the nonuniform structure formed on the surface of the neat Li electrode. The comparison of the galvanostatic cycling results of symmetric LiF-OC-Li/LiF-OC-Li cells and neat Li/Li cells demonstrated the effective promotion of cycle life of the lithium metal anode by LiF-OC coating, revealing that the fast lithium dendrite growth and formation of "dead lithium" were effectively mitigated.

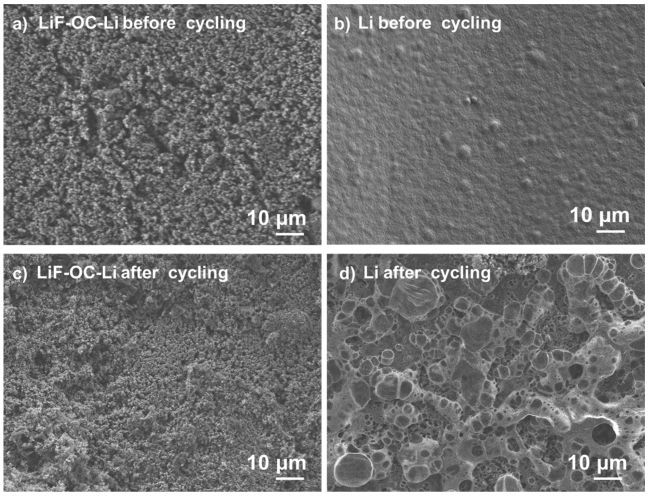

Figure 6. Comparison of the surface morphology of the (a) fresh Li-OC-Li, (b) fresh Li electrode, (c) LiF-OC-Li, and (d) neat Li after a 250 h stripping/plating test at a current density of 1 mA/cm^2.

To further quantitatively evaluate the LiF-OC-Li electrode, a Coulombic efficiency test was performed using a thin Li chip with a thickness of 50 μm as the working electrode. The LiF-OC-Li and neat Li were used as counter electrodes. The detailed cell setup and Coulombic efficiency (CE) calculation are described in the SI. A fixed amount of Li (0.5 mA h/cm^2) was stripped and plated at a current density of 4 mA/cm^2. The thin Li chips were assumed to be consumed when the overpotential exceeded 1.2 V, as shown in Figure S7. The Coulombic efficiency of the LiF-OC-Li electrode was determined to be 96.5%, while the neat Li electrode was determined with a Coulombic efficiency of 95.9%. The small

DOI: 10.1021/acsaem.9b01416
ACS Appl. Energy Mater. XXXX, XXX, XXX−XXX

improvement in CE is demonstrative of the improvement from the LiF-OC protection layer. It should be noted that the thin lithium electrode does not have a LiF-OC protection layer, but the CE calculation will include the efficiency loss of this thin Li electrode; thus, the increased CE with the LiF-OC-Li electrode is a lower bound. The similarity in voltage profiles (SI, Figure S7) in comparison to the profiles from symmetric cells (Figure 5) suggests that the performance for the CE measurement is strongly influenced by the thin Li chip.

4. CONCLUSIONS

In this work, an efficient and simple method was developed to fabricate modified Li electrodes (LiF-OC-Li) using microwave treatment to generate LiF from PVDF. Due to the selective heating of microwaves, the mesoporous onionlike carbon was rapidly heated to decompose the surrounding PVDF. Additionally, this heat provided sufficient energy to locally melt Li, and capillary forces drove the lithium metal to the interface. The Li reacted with the decomposition products from PVDF to form a LiF-rich passivation layer on the lithium metal electrode. The curved carbon layers facilitated the ion transport and minimized local potential variations, which in turn reduced the potential for fast dendrite growth. Concurrently, the LiF-rich surface layer provided high electrochemical stability and prevented erosion of the lithium anode through SEI formation. This enhanced stability of the modified Li was demonstrated by the impedance evolution, stable stripping/plating cycles in symmetric cells, as well as improved Coulombic efficiency over neat Li foil. With a stripping/plating capacity of 1 mA h/cm^2, the LiF-OC-Li electrode can be cycled over 1000 h at a current density of 0.5 mA/cm^2. As a comparison, the neat Li electrode failed after ~600 h. Even under higher current densities of 1 and 2 mA/cm^2, the LiF-OC-Li electrode can be cycled over 250 h. The neat Li electrode lost stability at ~150 and ~100 h, respectively. This methodology provides a novel, scalable concept for the fabrication of a stabilized lithium metal anode for rechargeable batteries.

■ ASSOCIATED CONTENT

Supporting Information

The Supporting Information is available free of charge on the ACS Publications website at DOI: 10.1021/acsaem.9b01416.

Experimental detail, computational detail, supporting analysis of BET, XPS, and a battery test (PDF)

■ AUTHOR INFORMATION

Corresponding Authors

*E-mail: bdv5051@psu.edu.

*E-mail: yu.zhu@uakron.edu.

ORCID

Bryan D. Vogt: 0000-0003-1916-7145

Yu Zhu: 0000-0002-2201-9066

Present Address

[‖]B.D.V.: Department of Chemical Engineering, The Pennsylvania State University, University Park, PA 16802, USA

Author Contributions

[§]K.L. and Y.X. contributed equally to this work. All authors have given approval to the final version of the manuscript.

Notes

The authors declare no competing financial interest.

■ ACKNOWLEDGMENTS

The authors are grateful for financial support from The University of Akron. The work was partially supported by the National Science Foundation (NSF) under Grants CBET-1706681 and CBET-1510612. This work used the Complex Materials Scattering (CMS/11-BM) beamline, operated by the National Synchrotron Light Source II and the Center for Functional Nanomaterials, which are U.S. Department of Energy (DOE) Office of Science User Facilities operated for the DOE Office of Science by Brookhaven National Laboratory under Contract DE-SC0012704.

■ REFERENCES

(1) Dunn, B.; Kamath, H.; Tarascon, J.-M. Electrical Energy Storage for the Grid: A Battery of Choices. *Science* **2011**, *334*, 928−935.

(2) Palacin, M. R.; de Guibert, A. Why Do Batteries Fail? *Science* **2016**, *351*, 1253292.

(3) Choi, J. W.; Aurbach, D. Promise and Reality of Post-Lithium-Ion Batteries with High Energy Densities. *Nat. Rev. Mater.* **2016**, *1*, 16013.

(4) Evarts, E. C. Lithium Batteries: To the Limits of Lithium. *Nature* **2015**, *526*, S93−S95.

(5) Tarascon, J. M.; Armand, M. Issues and Challenges Facing Rechargeable Lithium Batteries. *Nature* **2001**, *414*, 359−367.

(6) Armand, M.; Tarascon, J. M. Building Better Batteries. *Nature* **2008**, *451*, 652−657.

(7) Guo, Y.; Li, H.; Zhai, T. Reviving Lithium□Metal Anodes for Next□Generation High□Energy Batteries. *Adv. Mater.* **2017**, *29*, 1700007.

(8) Lin, D.; Liu, Y.; Cui, Y. Reviving The Lithium Metal Anode for High-Energy Batteries. *Nat. Nanotechnol.* **2017**, *12*, 194−206.

(9) Chan, C. K.; Peng, H.; Liu, G.; McIlwrath, K.; Zhang, X. F.; Huggins, R. A.; Cui, Y. High-Performance Lithium Battery Anodes Using Silicon Nanowires. *Nat. Nanotechnol.* **2008**, *3*, 31−35.

(10) Li, H.; Huang, X.; Chen, L.; Wu, Z.; Liang, Y. A High Capacity Nano-Si Composite Anode Material for Lithium Rechargeable Batteries. *Electrochem. Solid-State Lett.* **1999**, *2*, 547−549.

(11) Chan, C. K.; Zhang, X. F.; Cui, Y. High Capacity Li Ion Battery Anodes Using Ge Nanowires. *Nano Lett.* **2008**, *8*, 307−309.

(12) Poizot, P.; Laruelle, S.; Grugeon, S.; Dupont, L.; Tarascon, J. M. Nano-Sized Transition-Metal Oxides as Negative-Electrode Materials for Lithium-Ion Batteries. *Nature* **2000**, *407*, 496−499.

(13) Chen, J.; Xu, L.; Li, W.; Gou, X. α-Fe_2O_3 Nanotubes in Gas Sensor and Lithium□Ion Battery Applications. *Adv. Mater.* **2005**, *17*, 582−586.

(14) Mahmood, N.; Zhang, C.; Hou, Y. Nickel Sulfide/Nitrogen□Doped Graphene Composites: Phase□Controlled Synthesis and High Performance Anode Materials for Lithium Ion Batteries. *Small* **2013**, *9*, 1321−1328.

(15) OttakamThotiyl, M. M.; Freunberger, S. A.; Peng, Z.; Chen, Y.; Liu, Z.; Bruce, P. G. A Stable Cathode for The Aprotic Li−O_2 Battery. *Nat. Mater.* **2013**, *12*, 1050−1056.

(16) Liu, T.; Leskes, M.; Yu, W.; Moore, A. J.; Zhou, L.; Bayley, P. M.; Kim, G.; Grey, C. P. Cycling Li-O_2 Batteries *via*LiOH Formation and Decomposition. *Science* **2015**, *350*, 530−533.

(17) Bruce, P. G.; Freunberger, S. A.; Hardwick, L. J.; Tarascon, J.-M. Li−O_2 and Li−S Batteries with High Energy Storage. *Nat. Mater.* **2012**, *11*, 19−29.

(18) Wang, H.; Yang, Y.; Liang, Y.; Robinson, J. T.; Li, Y.; Jackson, A.; Cui, Y.; Dai, H. Graphene-Wrapped Sulfur Particles as a Rechargeable Lithium−Sulfur Battery Cathode Material with High Capacity and Cycling Stability. *Nano Lett.* **2011**, *11*, 2644−2647.

(19) Goodenough, J. B. Rechargeable Batteries: Challenges Old and New. *J. Solid State Electrochem.* **2012**, *16*, 2019−2029.

(20) Liu, J.; Bao, Z.; Cui, Y.; Dufek, E. J.; Goodenough, J. B.; Khalifah, P.; Li, Q.; Liaw, B. Y.; Liu, P.; Manthiram, A.; Meng, Y. S.; Subramanian, V. R.; Toney, M. F.; Viswanathan, V. V.; Whittingham,

DOI: 10.1021/acsaem.9b01416
ACS Appl. Energy Mater. XXXX, XXX, XXX−XXX

M. S.; Xiao, J.; Xu, W.; Yang, J.; Yang, X.-Q.; Zhang, J.-G. Pathways for Practical High-Energy Long-Cycling Lithium Metal Batteries. *Nat. Energy* **2019**, *4*, 180−186.
(21) Cheng, X.-B.; Peng, H.-J.; Huang, J.-Q.; Zhang, R.; Zhao, C.-Z.; Zhang, Q. Dual-Phase Lithium Metal Anode Containing a Polysulfide-Induced Solid Electrolyte Interphase and Nanostructured Graphene Framework for Lithium−Sulfur Batteries. *ACS Nano* **2015**, *9*, 6373−6382.
(22) Cheng, X. B.; Zhang, R.; Zhao, C. Z.; Zhang, Q. Toward Safe Lithium Metal Anode in Rechargeable Batteries: A Review. *Chem. Rev.* **2017**, *117*, 10403−10473.
(23) Zhang, X. Q.; Chen, X.; Cheng, X. B.; Li, B. Q.; Shen, X.; Yan, C.; Huang, J. Q.; Zhang, Q. Highly Stable Lithium Metal Batteries Enabled by Regulating the Solvation of Lithium Ions in Nonaqueous Electrolytes. *Angew. Chem., Int. Ed.* **2018**, *57*, 5301−5305.
(24) Ren, X.; Zhang, Y.; Engelhard, M. H.; Li, Q.; Zhang, J. G.; Xu, W. Guided Lithium Metal Deposition and Improved Lithium Coulombic Efficiency through Synergistic Effects of LiAsF6 and Cyclic Carbonate Additives. *ACS Energy Lett.* **2018**, *3*, 14−19.
(25) Yan, C.; Cheng, X. B.; Yao, Y. X.; Shen, X.; Li, B. Q.; Li, W. J.; Zhang, R.; Huang, J. Q.; Li, H.; Zhang, Q. An Armored Mixed Conductor Interphase on a Dendrite-Free Lithium-Metal Anode. *Adv. Mater.* **2018**, *30*, 1804461.
(26) Lopez, C. M.; Vaughey, J. T.; Dees, D. W. Morphological Transitions on Lithium Metal Anodes. *J. Electrochem. Soc.* **2009**, *156*, A726−A729.
(27) Lu, D.; Shao, Y.; Lozano, T.; Bennett, W. D.; Graff, G. L.; Polzin, B.; Zhang, J.; Engelhard, M. H.; Saenz, N. T.; Henderson, W. A.; Bhattacharya, P.; Liu, J.; Xiao, J. Failure Mechanism for Fast□Charged Lithium Metal Batteries with Liquid Electrolytes. *Adv. Energy Mater.* **2015**, *5*, 1400993.
(28) Zuo, T. T.; Yin, Y. X.; Wang, S. H.; Wang, P. F.; Yang, X.; Liu, J.; Yang, C. P.; Guo, Y. G. Trapping Lithium into Hollow Silica Microspheres with a Carbon Nanotube Core for Dendrite-Free Lithium Metal Anodes. *Nano Lett.* **2018**, *18*, 297−301.
(29) Zhang, X. Q.; Chen, X.; Xu, R.; Cheng, X. B.; Peng, H. J.; Zhang, R.; Huang, J. Q.; Zhang, Q. Columnar Lithium Metal Anodes. *Angew. Chem., Int. Ed.* **2017**, *56*, 14207−14211.
(30) Liu, L.; Yin, Y. X.; Li, J. Y.; Wang, S. H.; Guo, Y. G.; Wan, L. J. Uniform Lithium Nucleation/Growth Induced by Lightweight Nitrogen-Doped Graphitic Carbon Foams for High-Performance Lithium Metal Anodes. *Adv. Mater.* **2018**, *30*, 1706216.
(31) Khurana, R.; Schaefer, J. L.; Archer, L. A.; Coates, G. W. Suppression of Lithium Dendrite Growth Using Cross-Linked Polyethylene/Poly(ethylene oxide) Electrolytes: A New Approach for Practical Lithium-Metal Polymer Batteries. *J. Am. Chem. Soc.* **2014**, *136*, 7395−7402.
(32) Tu, Z. Y.; Nath, P.; Lu, Y. Y.; Tikekar, M. D.; Archer, L. A. Nanostructured Electrolytes for Stable Lithium Electrodeposition in Secondary Batteries. *Acc. Chem. Res.* **2015**, *48*, 2947−2956.
(33) Ko, J.; Yoon, Y. S. Recent Progress in LiF Materials for Safe Lithium Metal Anode of Rechargeable Batteries: Is LiF The Key to Commercializing Li Metal Batteries? *Ceram. Int.* **2019**, *45*, 30−49.
(34) Jia, W.; Fan, C.; Wang, L.; Wang, Q.; Zhao, M.; Zhou, A.; Li, J. Extremely Accessible Potassium Nitrate (KNO_3) as the Highly Efficient Electrolyte Additive in Lithium Battery. *ACS Appl. Mater. Interfaces* **2016**, *8*, 15399−15405.
(35) Wu, F.; Qian, J.; Chen, R.; Lu, J.; Li, L.; Wu, H.; Chen, J.; Zhao, T.; Ye, Y.; Amine, K. An Effective Approach To Protect Lithium Anode and Improve Cycle Performance for Li−S Batteries. *ACS Appl. Mater. Interfaces* **2014**, *6*, 15542−15549.
(36) Xiang, H.; Shi, P.; Bhattacharya, P.; Chen, X.; Mei, D.; Bowden, M. E.; Zheng, J.; Zhang, J.-G.; Xu, W. Enhanced Charging Capability of Lithium Metal Batteries Based on Lithium Bis-(trifluoromethanesulfonyl)imide-lithium Bis(oxalato)borate Dual-Salt Electrolytes. *J. Power Sources* **2016**, *318*, 170−177.
(37) Ye, H.; Yin, Y.-X.; Zhang, S.-F.; Shi, Y.; Liu, L.; Zeng, X.-X.; Wen, R.; Guo, Y.-G.; Wan, L.-J. Synergism of Al-containing Solid Electrolyte Interphase Layer and Al-based Colloidal Particles for Stable Lithium Anode. *Nano Energy* **2017**, *36*, 411−417.
(38) Li, W.; Yao, H.; Yan, K.; Zheng, G.; Liang, Z.; Chiang, Y.-M.; Cui, Y. The Synergetic Effect of Lithium Polysulfide and Lithium Nitrate to Prevent Lithium Dendrite Growth. *Nat. Commun.* **2015**, *6*, 7436.
(39) Zhao, C.-Z.; Cheng, X.-B.; Zhang, R.; Peng, H.-J.; Huang, J.-Q.; Ran, R.; Huang, Z.-H.; Wei, F.; Zhang, Q. Li_2S_5 Based Ternary-Salt Electrolyte for Robust Lithium Metal Anode. *Energy Storage Mater.* **2016**, *3*, 77−84.
(40) Yan, C.; Cheng, X.-B.; Zhao, C.-Z.; Huang, J.-Q.; Yang, S.-T.; Zhang, Q. Lithium Metal Protection Through *In-Situ* Formed Solid Electrolyte Interphase in Lithium-Sulfur Batteries: The Role of Polysulfides on Lithium Anode. *J. Power Sources* **2016**, *327*, 212−220.
(41) Zu, C.; Dolocan, A.; Xiao, P.; Stauffer, S.; Henkelman, G.; Manthiram, A. Breaking Down the Crystallinity: The Path for Advanced Lithium Batteries. *Adv. Energy Mater.* **2016**, *6*, 1501933.
(42) Zu, C.; Manthiram, A. High-Performance Li−S Batteries with an Ultra-lightweight MWCNT-Coated Separator. *J. Phys. Chem. Lett.* **2014**, *5*, 2522−2527.
(43) Murugan, R.; Thangadurai, V.; Weppner, W. Fast Lithium Ion Conduction in Garnet-Type $Li_7La_3Zr_2O_{12}$. *Angew. Chem., Int. Ed.* **2007**, *46*, 7778−7781.
(44) Yan, X.; Li, Z.; Wen, Z.; Han, W. $Li/Li_7La_3Zr_2O_{12}/LiFePO_4$ All-Solid-State Battery with Ultrathin Nanoscale Solid Electrolyte. *J. Phys. Chem. C* **2017**, *121*, 1431−1435.
(45) Zhao, Q.; Liu, X.; Stalin, S.; Khan, K.; Archer, L. A. Solid-State Polymer Electrolytes with In-Built Fast Interfacial Transport for Secondary Lithium Batteries. *Nat. Energy* **2019**, *4*, 365−373.
(46) Gao, Y.; Yan, Z.; Gray, J. L.; He, X.; Wang, D.; Chen, T.; Huang, Q.; Li, Y. C.; Wang, H.; Kim, S. H.; Mallouk, T. E.; Wang, D. Polymer-Inorganic Solid-Electrolyte Interphase for Stable Lithium Metal Batteries Under Lean Electrolyte Conditions. *Nat. Mater.* **2019**, *18*, 384−389.
(47) Li, S.; Chen, Y.-M.; Liang, W.; Shao, Y.; Liu, K.; Nikolov, Z.; Zhu, Y. A Superionic Conductive, Electrochemically Stable Dual-Salt Polymer Electrolyte. *Joule* **2018**, *2*, 1838−1856.
(48) Jiao, S.; Ren, X.; Cao, R.; Engelhard, M. H.; Liu, Y.; Hu, D.; Mei, D.; Zheng, J.; Zhao, W.; Li, Q.; Liu, N.; Adams, B. D.; Ma, C.; Liu, J.; Zhang, J.-G.; Xu, W. Stable Cycling of High-Voltage Lithium Metal Batteries in Ether Electrolytes. *Nat. Energy* **2018**, *3*, 739−746.
(49) Yamada, Y.; Yamada, A. Review—Superconcentrated Electrolytes for Lithium Batteries. *J. Electrochem. Soc.* **2015**, *162*, A2406−A2423.
(50) Zheng, J.; Lochala, J. A.; Kwok, A.; Deng, Z. D.; Xiao, J. Research Progress towards Understanding the Unique Interfaces between Concentrated Electrolytes and Electrodes for Energy Storage Applications. *Adv. Sci.* **2017**, *4*, 1700032.
(51) Ma, Q.; Fang, Z.; Liu, P.; Ma, J.; Qi, X.; Feng, W.; Nie, J.; Hu, Y.-S.; Li, H.; Huang, X.; Chen, L.; Zhou, Z. Improved Cycling Stability of Lithium□Metal Anode with Concentrated Electrolytes Based on Lithium (Fluorosulfonyl)(trifluoromethanesulfonyl)imide. *ChemElectroChem* **2016**, *3*, 531−536.
(52) Zhamu, A.; Chen, G.; Liu, C.; Neff, D.; Fang, Q.; Yu, Z.; Xiong, W.; Wang, Y.; Wang, X.; Jang, B. Z. Reviving Rechargeable Lithium Metal Batteries: Enabling Next-Generation High-Energy and High-Power Cells. *Energy Environ. Sci.* **2012**, *5*, 5701−5707.
(53) Zhang, Y.-J.; Xia, X.-H; Wang, D.-H.; Wang, X.-L.; Gu, C.-D.; Tu, J.-P. Integrated Reduced Graphene Oxide Multilayer/Li Composite Anode for Rechargeable Lithium Metal Batteries. *RSC Adv.* **2016**, *6*, 11657−11664.
(54) Cheng, X.-B.; Hou, T.-Z.; Zhang, R.; Peng, H.-J.; Zhao, C.-Z.; Huang, J.-Q.; Zhang, Q. Dendrite□Free Lithium Deposition Induced by Uniformly Distributed Lithium Ions for Efficient Lithium Metal Batteries. *Adv. Mater.* **2016**, *28*, 2888−2895.
(55) Raji, A.-R. O.; Salvatierra, R. V.; Kim, N. D.; Fan, X.; Li, Y.; Silva, G. A. L.; Sha, J.; Tour, J. M. Lithium Batteries with Nearly Maximum Metal Storage. *ACS Nano* **2017**, *11*, 6362−6369.

DOI: 10.1021/acsaem.9b01416
ACS Appl. Energy Mater. XXXX, XXX, XXX−XXX

(56) Hou, T.-Z.; Chen, X.; Peng, H.-J.; Huang, J.-Q.; Li, B.-Q.; Zhang, Q.; Li, B. Design Principles for Heteroatom□Doped Nanocarbon to Achieve Strong Anchoring of Polysulfides for Lithium−Sulfur Batteries. *Small* **2016**, *12*, 3283−3291.
(57) Kang, H.-K.; Woo, S.-G.; Kim, J.-H.; Lee, S.-R.; Kim, Y.-J. Conductive Porous Carbon Film as a Lithium Metal Storage Medium. *Electrochim. Acta* **2015**, *176*, 172−178.
(58) Yan, Z.; Wang, E.; Jiang, L.; Sun, G. Integrated Reduced Graphene Oxide Multilayer/Li Composite Anode for Rechargeable Lithium Metal Batteries. *RSC Adv.* **2015**, *5*, 83781−83787.
(59) Chi, S.-S.; Liu, Y.; Song, W.-L.; Fan, L.-Z.; Zhang, Q. Prestoring Lithium into Stable 3D Nickel Foam Host as Dendrite□Free Lithium Metal Anode. *Adv. Funct. Mater.* **2017**, *27*, 1700348.
(60) Zhang, X.; Wang, W.; Wang, A.; Huang, Y.; Yuan, K.; Yu, Z.; Qiu, J.; Yang, Y. Improved Cycle Stability and High Security of Li-B Alloy Anode for Lithium−Sulfur Battery. *J. Mater. Chem. A* **2014**, *2*, 11660−11665.
(61) Cheng, X.-B.; Peng, H.-J.; Huang, J.-Q.; Wei, F.; Zhang, Q. Dendrite□Free Nanostructured Anode: Entrapment of Lithium in a 3D Fibrous Matrix for Ultra□Stable Lithium−Sulfur Batteries. *Small* **2014**, *10*, 4257−4263.
(62) Peng, Z.; Zhao, N.; Zhang, Z.; Wan, H.; Lin, H.; Liu, M.; Shen, C.; He, H.; Guo, X.; Zhang, J.-G.; Wang, D. Stabilizing Li/Electrolyte Interface with a Transplantable Protective Layer Based on Nanoscale LiF Domains. *Nano Energy* **2017**, *39*, 662−672.
(63) Xie, J.; Liao, L.; Gong, Y.; Li, Y.; Shi, F.; Pei, A.; Sun, J.; Zhang, R.; Kong, B.; Subbaraman, R.; Christensen, J.; Cui, Y. Stitching h-BN by Atomic Layer Deposition of LiF as a Stable Interface for Lithium Metal Anode. *Sci. Adv.* **2017**, *3*, No. eaao3170.
(64) Zhao, J.; Liao, L.; Shi, F.; Lei, T.; Chen, G.; Pei, A.; Sun, J.; Yan, K.; Zhou, G.; Xie, J.; Liu, C.; Li, Y.; Liang, Z.; Bao, Z.; Cui, Y. Surface Fluorination of Reactive Battery Anode Materials for Enhanced Stability. *J. Am. Chem. Soc.* **2017**, *139*, 11550−11558.
(65) Gu, D.; Bongard, H.; Deng, Y. H.; Feng, D.; Wu, Z. X.; Fang, Y.; Mao, J. J.; Tu, B.; Schuth, F.; Zhao, D. Y. An Aqueous Emulsion Route to Synthesize Mesoporous Carbon Vesicles and Their Nanocomposites. *Adv. Mater.* **2010**, *22*, 833−837.
(66) Meng, Y.; Gu, D.; Zhang, F.; Shi, Y.; Cheng, L.; Feng, D.; Wu, Z.; Chen, Z.; Wan, Y. A.; Stein, Y.; Zhao, D. A Family of Highly Ordered Mesoporous Polymer Resin and Carbon Structures from Organic-Organic Self-Assembly. *Chem. Mater.* **2006**, *18*, 4447−4464.
(67) Yoshikawa, N. Fundamentals and Applications of Microwave Heating of Metals. *J. Microw. Power and Electromagn. Energy* **2010**, *44*, 4−13.
(68) Menéndez, J. A.; Arenillas, A.; Fidalgo, B.; Fernández, Y.; Zubizarreta, L.; Calvo, E. G.; Bermúdez, J. M. Microwave Heating Processes Involving Carbon Materials. *Fuel Process. Technol.* **2010**, *91*, 1−8.
(69) Meng, X.-M.; Zhang, X.-J.; Lu, C.; Pan, Y.-F.; Wang, G.-S. Enhanced Absorbing Properties of Three-Phase Composites Based on a Thermoplastic-Ceramic Matrix ($BaTiO_3$ + PVDF) and Carbon Black Nanoparticles. *J. Mater. Chem. A* **2014**, *2*, 18725−18730.
(70) Bodenes, L.; Darwiche, A.; Monconduit, L.; Martinez, H. The Solid Electrolyte Interphase a Key Parameter of The High Performance of Sb in Sodium-Ion Batteries: Comparative X-ray Photoelectron Spectroscopy Study of Sb/Na-Ion and Sb/Li-Ion Batteries. *J. Power Sources* **2015**, *273*, 14−24.
(71) Wood, K. N.; Steirer, K. X.; Hafner, S. E.; Ban, C.; Santhanagopalan, S.; Lee, S.-H.; Teeter, G. Operando X-Ray Photoelectron Spectroscopy of Solid Electrolyte Interphase Formation and Evolution in Li_2S-P_2S_5 solid-state electrolytes. *Nat. Commun.* **2018**, *9*, 2490.
(72) Lin, D.; Liu, Y.; Chen, W.; Zhou, G.; Liu, K.; Dunn, B.; Cui, Y. Conformal Lithium Fluoride Protection Layer on Three-Dimensional Lithium by Nonhazardous Gaseous Reagent Freon. *Nano Lett.* **2017**, *17*, 3731−3737.
(73) Cheng, X.-B.; Zhang, R.; Zhao, C.-Z.; Zhang, Q. Toward Safe Lithium Metal Anode in Rechargeable Batteries: A Review. *Chem. Rev.* **2017**, *117*, 10403−10473.
(74) Ye, H.; Xin, S.; Yin, Y.-X.; Li, J.-Y.; Guo, Y.-G.; Wan, L.-J. Stable Li Plating/Stripping Electrochemistry Realized by a Hybrid Li Reservoir in Spherical Carbon Granules with 3D Conducting Skeletons. *J. Am. Chem. Soc.* **2017**, *139*, 5916−5922.

DOI: 10.1021/acsaem.9b01416
ACS Appl. Energy Mater. XXXX, XXX, XXX−XXX